https://doi.org/10.5194/hess-2024-51
Preprint. Discussion started: 13 March 2024

Hydrology and Earth System Sciences
Discussions
Open Access
EGU

On the Influence of Spatial Heterogeneity of Runoff Generation on the Distributed Unit Hydrograph for Flood Prediction

Bin Yi[1,2], Lu Chen[1,2,3]*, Tao Xie[1,2]

1. *School of Civil and Hydraulic Engineering, Huazhong University of Science and Technology, Wuhan, 430074, China*

2. *Hubei Key Laboratory of Digital Valley Science and Technology, Wuhan 430074, China*

3. *School of Water Resources and Civil Engineering, Tibet Agricultural & Animal Husbandry University, Linzhi 860000, China*

Correspondence: Lu Chen (chen_lu@hust.edu.cn)

Abstract: The spatial scale mismatch between runoff generation and runoff routing is an acceptable compromise but a common issue in challenging hydrological modelling. Moreover, there is hardly any report available on whether unit hydrograph (UH) that is consistent with the spatial scale of runoff generation can be computed. The objective of this study was to explore the influence of spatial heterogeneity of runoff generation on the UH for flood prediction. To this end, a novel GIS-based dynamic time-varying unit hydrograph (DTDUH) was proposed based on the time-varying unit hydrograph (TDUH). The DTDUH can be defined as a typical hydrograph of direct runoff which gets generated from one centimeter of effective rainfall falling at a uniform rate over the saturated drainage basin uniformly during a specific duration. The DTDUH was computed based on the saturated areas of the watershed instead of the global watershed. The saturated areas were extracted based on the TWI. Finally, the Longhu River basin and Dongshi River basin were selected as two case studies. Results showed that the proposed method exhibited consistent or better performance compared with that of the linear reservoir routing method, and performed better than the TDUH method. Specifically, the DTDUH method indicated good performances for the flood events with low antecedent soil moisture, and it performed consistently with the TDUH when the global watershed is nearly saturated. The

https://doi.org/10.5194/hess-2024-51
Preprint. Discussion started: 13 March 2024


Hydrology and Earth System Sciences
Discussions
Open Access
EGU

proposed method can be used for the watersheds with sparse gauging stations and limited observed rainfall and runoff data, as is the same with the TDUH method. Simultaneously, it is well applicable for the humid or mountain watershed where the saturation-excess rainfall is the dominant.

Keywords: Hydrological modelling; Distributed unit hydrograph; Runoff routing; Runoff generation; XAJ model

1. Introduction

The assumption that basins behave as linear systems (i.e., there is proportionality and additivity between excess rainfall and total storm response) has been the core to hydrology over the past century (Goodrich et al., 1997; Bunster et al., 2019). On such condition, a single response function named the UH has been widely applied to acquire the stormflow at the basin outlet (Czyzyk et al., 2020). The UH can be developed for both gauged and ungauged watersheds (Monajemi et al., 2021). For gauged basins, unit hydrographs are derived from observed data by measuring rainfall and runoff data. For ungauged basin, some synthetic methods, such as the Snyder's method (Snyder, 1938) and Gray's method (Gray, 1961), are used to determine the unit hydrographs from spatially averaged basin characteristics. One variation is the synthetic UH method proposed by Clark (1945), in which the UH was derived by integrating two basic features of a watershed rainfall-runoff process. Specifically, translation through water movement was characterized by time-area method, and linear reservoir routing was used to represent attenuation through storage (Cho et al., 2018; Bunster et al., 2019). This history of development was synthetized in the works of Rodríguez-Iturbe and Valdés (1979) and Gupta et al. (1980), who proposed the geomorphological instantaneous unit hydrograph (GIUH). Subsequently, the width function-based geomorphological instantaneous unit hydrograph (WFIUH) method has been

https://doi.org/10.5194/hess-2024-51
Preprint. Discussion started: 13 March 2024


Hydrology and Earth System Sciences
Discussions
Open Access
EGU

formulated with the development of digital elevation models (DEMs) and geographic information system (GIS) technology (Seo et al., 2016). The WFIUH was derived by combining the flow paths to the outlet given by the width function with the flow celerity along the flow paths (Kirkby, 1976).

The UH method assumes the watershed response to be linear and time invariant, and rainfall to be spatially homogeneous. In contrast to the linearity assumption, basins have been shown to exhibit nonlinearity in the transformation of excess rainfall to stormflow (Bunster et al., 2019). For a small watershed, Minshall (1960) showed that significantly different UHs were produced by different rainfall intensities. To cope with this nonlinearity, Rodríguez-Iturbe et al. (1982) extended the GIUH to the geomorphoclimatic IUH (GcIUH) by incorporating excess rainfall intensity. Lee et al. (2008) proposed a variable kinematic wave GIUH accounting for time-varying rainfall intensity, which may be applicable to ungauged catchments that are influenced by high intensity rainfall. To this end, it is necessary to consider the geomorphic characteristics of the watershed and incorporate time-varying rainfall intensity in the rainfall-runoff modelling processes.

Spatially distributed travel time models, also known as Spatially Distributed Unit Hydrograph models (DUH) (Maidment et al., 1996), are a semi-analytical form of the WFIUH identified by Rigon et al. (2016) in which spatially distributed flow celerity associated with the watershed characteristics and temporally varying excess rainfall rates can be considered. In this method, the travel time of each grid cell can be calculated by dividing the travel distance of a cell to the next cell by the velocity of flow generated in that cell (Paul et al., 2018). The travel time is then summed along the flow path to obtain the total travel time from each cell to the outlet. The DUH is thus derived using the distribution of travel time from all grid cells in a watershed. Several aspects (i.e. Rainfall intensities, upstream

https://doi.org/10.5194/hess-2024-51
Preprint. Discussion started: 13 March 2024


Hydrology and Earth System Sciences
Discussions

contributions, watershed equilibrium) were attracted much attention to obtain more accurate travel time distributions. Some DUH methods assumed a time-invariant travel time field and ignored the dependence of travel time on excess rainfall intensity (Melesse and Graham, 2004; Noto and La Loggia, 2007; Gibbs et al., 2010; Grimaldi et al., 2010), while others suggested various UHs corresponding to different storm events, namely time-varying distributed unit hydrograph (TDUH) (Martinez et al., 2002; Sarangi et al., 2007; Du et al., 2009). The upstream contributions to the travel time estimation should also been considered in the time-varying DUH method, which was developed from a static upstream contribution to a dynamic contribution. For example, Bunster et al. (2019) developed a TDUH model that accounts for dynamic upstream contributions and compared its performance against other TDUH methods, and characterized the temporal behavior of upstream contributions and its impact on travel times in the basin. However, the methods discussed above assumed that equilibrium in each individual grid cell or global watershed can be reached before the end of the rainfall excess pulse. To this end, Yi et al. (2022) proposed a time-varying distributed unit hydrograph method for runoff routing that accounts for dynamic rainfall intensity and soil moisture content, namely the time-varying distributed unit hydrograph considering soil moisture content (TDUH-MC). Hydrologists have made great efforts to address the nonlinear issues of the UHs in the past decades, while these approximations are still acceptable compromises in challenging hydrology research.

Nevertheless, we found that these approximations discussed above neglected the influence of spatial heterogeneity of runoff generation on the UH. For instance, in a humid watershed, the excess rainfall can be more inclined to happen at near-channel areas, and sometimes in the arid zones with long-storms duration according to the saturation-excess mechanism (Li and Sivapalan, 2014). In

https://doi.org/10.5194/hess-2024-51
Preprint. Discussion started: 13 March 2024


Hydrology and Earth System Sciences
Discussions

previous studies, the time-varying rainfall intensities were commonly considered to obtain a more accurate travel time distributions to compute the UH for the whole basin, while the depth of the excess rainfall was also considered to be uniformly distributed throughout the whole watershed (the excess rainfall actually comes from local saturated areas). The outflow hydrograph is then calculated by superimposing the response to each individual excess rainfall pulse, or equivalently by convoluting the spatially averaged excess rainfall and a UH obtained from the IUH. This indeed raised a problem that whether the unit hydrograph can reflect the realities of the runoff routing processes of an actual watershed.

The problem of spatial scale mismatch between runoff generation and confluence theory is prevalent in hydrological modeling, and hydrologists almost ignore the forecasting errors associated with this issue. For example, the Xinanjiang (XAJ) model is a conceptual hydrological model proposed by Zhao et al. (1980) for flood forecasts in the Xin'an River basin. It has been widely used in humid and semi-humid watersheds all over the world (Zhao, 1992; Zhou et al., 2019; Huang et al., 2020). In the model, two parabolic curves are adopted to represent the spatially non-uniform distribution of the tension water storage and the free water storage. In order to match the spatial scales of the runoff generation and the runoff routing, the excess rainfall generated in the saturated areas was assumed to be uniformly distributed across the whole basin. However, this assumption may result in huge errors, and there is hardly any report available on whether UH that is consistent with the spatial scale of runoff generation can be computed.

The objective of this study was therefore to explore the influence of spatial heterogeneity of runoff generation on the UH for flood prediction. The main contributions of the present study are given as

https://doi.org/10.5194/hess-2024-51
Preprint. Discussion started: 13 March 2024

follows. 1) The DUH method was used as the basic tool to compute the DTDUH corresponding to various saturated states of the watershed. 2) The definition of the DTDUH was different with the traditional TDUH as it represented the characteristics of the runoff generated areas instead of the whole basin. 3) The XAJ model was used as the hydrological modelling framework to unify the spatial scales of the runoff generation and the confluence method. The performance of the DTDUH method was compared with that of the traditional TDUH method based on flood events. Finally, the Longhu River basin and the Dongshi River basin in the Guangdong Province, China, were selected as two case studies. The influence of spatial heterogeneity of runoff generation on the UH for flood prediction was investigated.

2. Hydrological models

2.1 Runoff generation based on the saturation-excess mechanism

Saturation-excess runoff is the major runoff mechanism in humid well-vegetated areas where infiltration rates often exceed rainfall intensity (Tromp-Van Meerveld and McDonnell, 2006; Hoang et al., 2017). Many hydrological models, such as the TOPMODEL (Beven and Kirkby, 1979), the Variable Infiltration Capacity (VIC) model (Liang et al., 1994), the Probability Distributed Model (PDM) (Moore, 2007), the XAJ model (Zhao, 1992), and the Australian Water Balance Model (Boughton, 2004), simulate saturation-excess runoff by introducing a statistical distribution of tension water storage capacity using different methods. Simultaneously, a free water capacity distribution curve is usually used to divide the total runoff into the surface runoff, interflow and groundwater. In the XAJ model, two parabolic curves are adopted to represent the spatially non-uniform distribution of the tension water storage and free water storage. The functional relationships of the tension water

https://doi.org/10.5194/hess-2024-51
Preprint. Discussion started: 13 March 2024


Hydrology and Earth System Sciences
Discussions
Open Access
EGU

129 storage capacity curve and free water storage capacity are given by

130 $$\frac{A_{ps}}{A_p} = 1 - \left(1 - \frac{W}{WMM}\right)^{B} \quad (1)$$

131 $$\frac{A_f}{A_s} = 1 - \left(1 - \frac{S}{SMM}\right)^{EX} \quad (2)$$

132 where A_{ps} is the partial pervious area where the tension water storage capacity is less than or equal
133 to the value *W,* which is the tension water capacity at a point, varying from 0 to a maximum *WMM*;
134 A_p is the pervious area of the catchment; B is the exponential of distribution of the tension water
135 capacity; A_f is the area where the free water storage capacity is less than or equal to the value *S*,
136 varying from 0 to *SMM*; A_s is the runoff generation area; and *EX* is the exponential of distribution of
137 the free water storage capacity curve.

138 Based on Eq. (1), when rainfall exceeds evaporation, the runoff generated in the saturated areas
139 can be expressed by

140 $$R = \begin{cases} PE - WM + W_0 + WM\left(1 - \dfrac{PE + AU}{WMM}\right)^{1+B} & PE + AU < WMM \\ PE - WM + W_0 & PE + AU \geq WMM \end{cases} \quad (3)$$

141 where *R* is the total runoff (mm); *WM* is the areal mean tension water capacity (mm); *PE* is the rainfall
142 which exceeds evaporation (mm); W_0 is the initial areal mean tension water storage (mm); *AU* is the
143 vertical coordinate corresponding to W_0.

144 The total runoff *R*, generated in a wet period in accordance with Eq. (3), can be subsequently
145 separated into three components, including the surface runoff, interflow and groundwater (Zhao, 1992).

146 $$RS = \begin{cases} FR\left[PE + S - SM + SM\left(1 - \dfrac{PE + BU}{MS}\right)^{1+EX}\right] & PE + BU < SMM \\ FR\left(PE + S - SM\right) & PE + BU \geq SMM \end{cases} \quad (4)$$

https://doi.org/10.5194/hess-2024-51
Preprint. Discussion started: 13 March 2024

Hydrology and Earth System Sciences
Discussions

$$RI = KI \cdot S \cdot FR \tag{5}$$

$$RG = KG \cdot S \cdot FR \tag{6}$$

where *RS*, *RI*, *RG* represent the depth of the surface runoff, interflow and groundwater respectively (mm); *FR*, equalling to R/PE, is the proportion of the runoff producing area over the whole basin; *SM* is the areal mean free water capacity (mm); *BU* is the vertical coordinate corresponding to *S* (mm); and *KI* and *KG* are outflow coefficients of the free water storage to interflow and groundwater, respectively.

2.2 Derivation of the DTDUH for the surface runoff routing

The GIS-derived DUH method was employed for the surface runoff routing calculations, which allowed the velocity to be calculated on a grid cell basis over the watershed. To remove the linearity assumption, fully distributed models use routing methods which are usually computationally intensive because they solve the St. Venant equations (Bunster et al., 2019), so they are usually limited to small basins. Therefore, the DUH method is an alternative method that allows the use of distributed information in a much more efficient manner. The TDUH method was used for the computation of the UH, which considered both the time-varying rainfall intensities and the soil moisture. More details can be found in Yi et al. (2022). The DTDUH proposed in this study are computed based on the TDUH. The schematic diagram of the DTDUH method is shown in Fig. 1.

https://doi.org/10.5194/hess-2024-51
Preprint. Discussion started: 13 March 2024

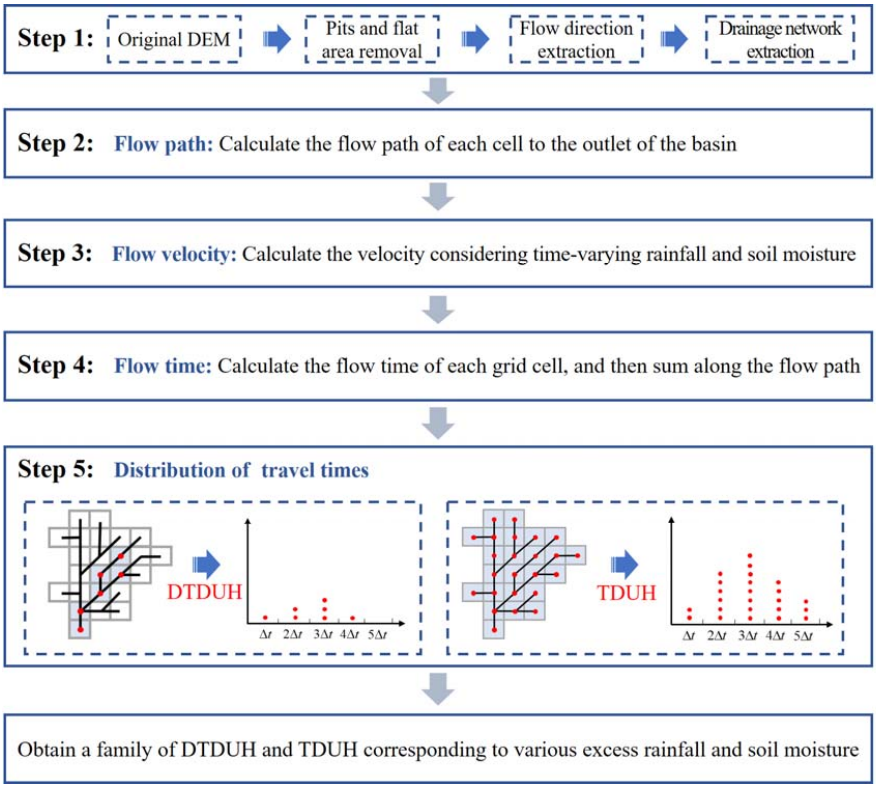

Figure 1. Schematic diagram of the DTDUH method. The main differences between the DTDUH and TDUH lie in that the DTDUH is computed based on local areas while the TDUH is for the global watershed.

1) The drainage network can be identified based on the advanced DEM preprocessing method (Grimaldi et al., 2012). Then, the flow path collection ($\mathbf{Road}_{A_j}$) of each gird cell A_j along the flow directions to the basin outlet can be created. For the whole basin, the flow path collection of all the grid cells ($\mathbf{Road}$) is expressed by

$$\mathbf{Road} = \left\{ \mathbf{Road}_{A_j} \middle| A_j \in \mathbf{A} \right\} \tag{7}$$

where A_j ($j = 1, 2, \cdots, N$) is the grid cell, N is the total grid cells of the basin; and $\mathbf{A}$ is the collection of all the grid cell.

https://doi.org/10.5194/hess-2024-51
Preprint. Discussion started: 13 March 2024


Hydrology and Earth System Sciences
Discussions

175 The depth of the excess rainfall occurs only in the saturated areas when the entire basin does not
176 reach a global saturated state, while current methods compute the DUH corresponding to the whole
177 basin. To this end, we proposed to create a collection of flow paths for the saturated areas, and the
178 specific formula is given by

179 $$\mathbf{Road}_{\alpha} = \left\{ \mathbf{Road}_{A_j} \middle| A_j \in \mathbf{A}_{\alpha} \right\} \tag{8}$$

180 where $\mathbf{Road}_{\alpha}$ ($\mathbf{Road}_{\alpha} \subseteq \mathbf{Road}$) is the flow path collection of the saturated grid cells when the soil
181 moisture proportion is α; and $\mathbf{A}_{\alpha}$ is the collection of the saturated grid cells when the soil moisture
182 proportion is α.

183 2) The flow velocity of each grid cell corresponding to the collection $\mathbf{Road}_{\alpha}$ is computed based
184 on the watershed characteristics and the spatial-temporal distribution characteristics of rainfall and soil
185 moisture, and the specific formula is given as Eq. (9) (Yi et al., 2022).

186 $$V = k \cdot S^{\frac{1}{2}} \cdot \left(\frac{I_t}{I_c} \right)^{\frac{2}{5}} \cdot (\alpha_t)^{\gamma} \tag{9}$$

187 where V (m s^{-1}) is the flow velocity; k (m s^{-1}) is the land use or flow type coefficient, S (m m^{-1}) is the
188 slope of the grid cell; I_t (mm h^{-1}) is the excess rainfall intensity at time t; I_c is the reference excess
189 rainfall intensity of the basin; α_t (unitless) represents the soil moisture content of the basin at time t;
190 and γ (unitless) is an exponent smaller than unity, which represents the nonlinear relationship
191 between soil moisture content and flow velocity.

192 3) The travel time for each grid cell in collection $\mathbf{Road}_{\alpha}$ can be calculated by Eq. (10). To
193 compute the total travel time τ_i of flow from each cell i to the outlet, travel times along the R_i cells
194 belonging to the flow path that starts at that cell are added based on Eq. (11).

https://doi.org/10.5194/hess-2024-51
Preprint. Discussion started: 13 March 2024


Hydrology and Earth System Sciences
Discussions

$$\Delta\tau_j = \frac{L_j}{V} \quad \text{or} \quad \Delta\tau_j = \frac{\sqrt{2}L_j}{V} \tag{10}$$

$$\tau_j = \sum_{A_j \in \mathbf{A}_\alpha} \Delta\tau_j \tag{11}$$

where $\Delta\tau_j$ is the retention time in grid cell A_j; τ_j is the total travel time along the flow path for grid cell A_j; L_j is the grid cell size. When the rasterized flow is flowing along the edges of the grid cell, the travel length is the cell size L_j, whereas the travel length is $\sqrt{2}L_j$ when it is flowing diagonally.

4) Develop a cumulative travel time map of the saturated areas instead of the whole basin based on cell-by-cell estimates for hillslope velocities. The cumulative travel time map is further divided into isochrones, which can be used to generate a time-area curve and the resulting DTDUH corresponding to the collection $\mathbf{Road}_\alpha$ instead of $\mathbf{Road}$.

2.3 Hydrological modelling framework

The XAJ model proposed by Zhao et al. (1980) was used as the hydrological modelling framework. It has been widely used in humid and semi-humid watersheds all over the world. There are four modules in the model including the evapotranspiration module, runoff generation module, runoff partition module and runoff routing module. For the evapotranspiration module, the soil profile of each sub-basin is divided into three layers, the upper, lower and deeper layers, and only when water in the layer above it has been exhausted does evaporation from the next layer occur. For the runoff generation and runoff partition modules in the XAJ model, they have been reviewed in Section 2.1. Finally, for the runoff routing module, subsurface stormflow and subsurface runoff were considered using a free reservoir. To compare the differences of spatial scale mismatch between the runoff generation and the runoff routing, linear reservoir, TDUH and DTDUH were selected as the surface runoff routing methods. The Muskingum method was employed to produce streamflow from channel

https://doi.org/10.5194/hess-2024-51
Preprint. Discussion started: 13 March 2024

Hydrology and Earth System Sciences
Discussions
Open Access
EGU

216 to the outlet of the entire basin. The XAJ modelling framework used in this study is given in Fig. 2.

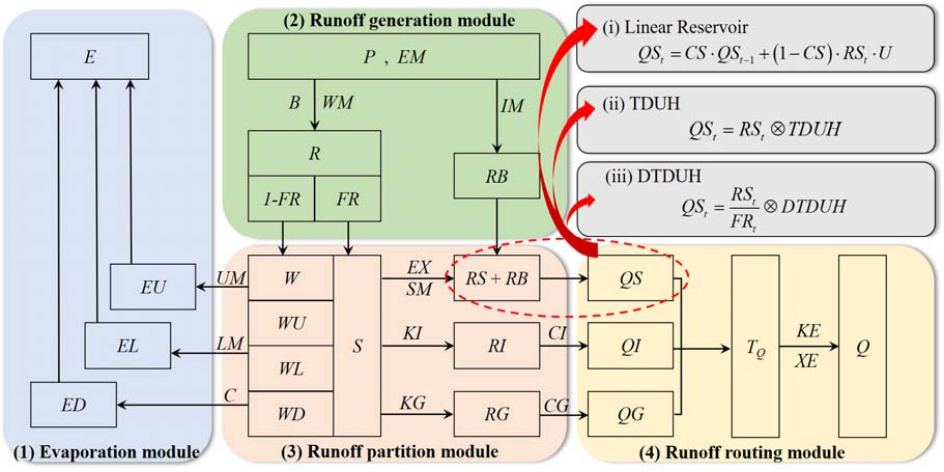

217

218 **Figure 2.** Schematic diagram of the XAJ model.

219 The depths of the surface runoff calculated by Eq. (4) are obtained after a redistribution to the
220 whole basin. As a matter of fact, the depths of the surface runoff should be calculated only over the
221 saturated areas when the DTDUH was selected as the surface runoff routing method, which can be
222 expressed by

223 $$RS_s^{'} = \frac{RS_s}{FR} \tag{12}$$

224 where $RS_s^{'}$ is the depth of the surface runoff corresponding to the saturated areas.

225 When the linear reservoir, TDUH and DTDUH were used respectively for the surface runoff
226 routing, the flow discharge at the outlet of the watershed can be computed by

227 $$QS_t = CS \cdot QS_{t-1} + (1-CS) \cdot RS_t \cdot \frac{F}{3.6\Delta t} \tag{13}$$

228 $$QS_t = RS_t \otimes TDUH \tag{14}$$

229 $$QS_t = RS_t^{'} \otimes DTDUH \tag{15}$$

230 where CS is the recession constant of the surface water storage; F (km^2) is the area of the basin, and

https://doi.org/10.5194/hess-2024-51
Preprint. Discussion started: 13 March 2024

231 $\otimes$ is the symbol of convolution.

232 *2.4 Model calibration and evaluation*

233 The Shuffled Complex Evolution Algorithm (SCE-UA) technique was developed by the
234 University of Arizona in 1992 for nonlinear, high dimensional optimization issues (Duan et al., 1992).
235 The technique has been used extensively for calibrating hydrological models (Zhou et al., 2019).
236 Consequently, the SCE-UA method was employed in this study to optimize the parameters of the
237 hydrological model. An aggregated objective function made up of three measures and aimed at
238 maximizing flow characteristics was used for the parameter calibration (Brunner et al., 2021; Yi et al.,
239 2022; Yi et al., 2023). The aggregated objective function and three metrics are expressed by

240 $$E_{\mathrm{NS}}=1-\frac{\sum_{t=1}^{T}\left|Q_s^t-Q_o^t\right|}{\sum_{t=1}^{T}\left|Q_o^t-\overline{Q_o}\right|} \tag{16}$$

241 $$E_{\mathrm{KG}}=1-\sqrt{(r-1)^2+\left(\frac{\sigma_s}{\sigma_o}-1\right)^2+\left(\frac{\mu_s}{\mu_o}-1\right)^2} \tag{17}$$

242 $$R_{\mathrm{SR}}=\sqrt{\frac{\sum_{t=1}^{T}\left(Q_o^t-Q_s^t\right)^2}{\sum_{t=1}^{T}\left(Q_o^t-\overline{Q_o}\right)^2}} \tag{18}$$

243 $$M=0.5\times\left(1-E_{\mathrm{NS}}\right)+0.25\times\left(1-E_{\mathrm{KG}}\right)+0.15\times\left(1-\log\left(E_{\mathrm{NS}}\right)\right)+0.1\times R_{\mathrm{SR}} \tag{19}$$

244 where Q_o^t is the observed discharge at time t; Q_s^t is the simulated discharge at time t; $\overline{Q_o}$ is the
245 mean of the observed discharge; T is the duration of the flood event; r is the correlation coefficient
246 between the observed and simulated flood; σ_s and σ_o are the standard deviation values for the simulated
247 and observed responses, respectively; and μ_s and μ_o are the corresponding mean values.

248 Several criteria were used for the model performance evaluation, consisting of the E_{NS}, the Root
249 Mean Square Error (*RMSE*), the relative flood peak error (Q_{P}) and the flood peak time error (T_{P}), which
250 can be expressed by

251 $$RMSE=\sqrt{\frac{1}{T}\sum_{t=1}^{T}\left(Q_s^t-Q_o^t\right)^2} \tag{20}$$

https://doi.org/10.5194/hess-2024-51
Preprint. Discussion started: 13 March 2024

$$Q_p = \frac{Q_p^s - Q_p^o}{Q_p^o} \tag{21}$$

$$T_p = T_p^s - T_p^o \tag{22}$$

where Q_p^s is the simulated flood peak discharge; Q_p^o is the observed flood peak discharge; T_p^o is the observed flood peak time; and T_p^s is the simulated flood peak time.

3. Study area and data

The Longhu River basin and the Dongshi River basin were selected as two case study watersheds. The Longhu river and the Dongshi river are located in the humid mountain area, which originate from the Hanjiang River basin of the Guangdong Province, China. The Longhu river is 17.4 km long, with a basin area of 102.7 km^2, and the mean slope of the basin is 2.9 ‰. The Dongshi river is 23.6 km long, with a basin area of 152.4 km^2, and the mean slope of the basin is 3.56 ‰. The DEM data of the two basins were collected from (http://www.gscloud.cn/). The land cover data can be accessed from (http://data.ess.tsinghua.edu.cn/). The distributions of the DEM, slope and land cover for the two basins are shown in Fig. 3.

https://doi.org/10.5194/hess-2024-51
Preprint. Discussion started: 13 March 2024

Hydrology and Earth System Sciences
Discussions
Open Access
EGU

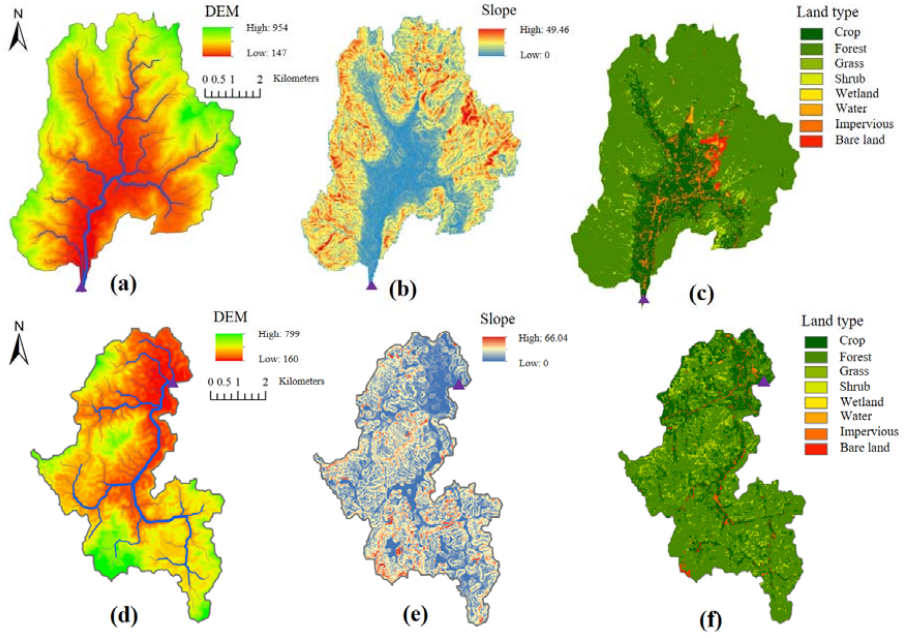

265

266 **Figure 3.** Distribution of the DEM, slope and land cover. (a), (b) and (c) are the DEM, slope and land
267 cover corresponding to the Dongshi River basin. (d), (e) and (f) are the DEM, slope and land cover
268 corresponding to the Longhu River basin.

269 Additionally, the rainfall and evaporation data from meteorological stations for the two basins
270 were collected from 1973 to 2020, and the simultaneous hourly runoff data for the outlet of the
271 watersheds were collected as well. A total of 32 isolated storms with the observed runoff responses
272 from 1973 to 2020 were selected to calibrate and verify the established model. The Dongshi
273 hydrological station was built in recent years, and the flow sequences were therefore short. Specifically,
274 16 flood events in the Longhu River basin with 1 hour interval were collected from 1973 to 2016, and
275 16 flood events with 1 hour interval were collected from the Dongshi River basin from 2015 to 2020.
276 The statistics of these flood events are shown in Table 1. The average flood peaks for the Longhu River

https://doi.org/10.5194/hess-2024-51
Preprint. Discussion started: 13 March 2024

Hydrology and Earth System Sciences
Discussions

basin and the Dongshi River basin are 116.7 $m^3 s^{-1}$ and 73.0 $m^3 s^{-1}$, respectively. The average flood durations are about 30 h and 33 h, respectively. Moreover, to consider the initial condition, the antecedent precipitation was calculated based on the daily recession coefficient of the water storage.

Table 1. Statistics of the flood events in the Longhu and the Dongshi River basins.

Watershed	Flood events	Rainfall (mm)	Flood peak (m^3 s^{-1})	Time duration (h)
Longhu	19730508	80.0	94.5	27
	19730720	76.7	180.0	17
	19750526	54.9	101.0	21
	19760702	73.0	137.0	28
	19770526	73.8	90.4	18
	19771003	62.1	97.5	19
	19790607	100.3	93.4	24
	19890502	46.5	132.0	29
	20030517	94.0	140.0	46
	20060601	56.0	96.5	37
	20120527	118.8	128.0	27
	20130713	214.4	228.0	30
	20150601	83.4	85.0	44
	20150831	102.6	83.2	30
	20160430	111.2	91.0	54
	20160903	85.4	89.7	26
Dongshi	20150509	105.2	62.9	38
	20150721	132.0	82.0	29
	20160811	90.0	51.3	48
	20160819	112.5	34.9	19
	20161021	158.8	48.0	49
	20170501	84.5	98.3	22
	20170515	84.0	43.7	29
	20170613	139.2	37.2	31
	20170929	71.0	101.2	25
	20180606	61.5	34.9	32
	20180702	23.5	44.3	25
	20190418	86.4	35.5	18
	20190609	107.6	272.0	27
	20190612	74.0	100.0	66
	20200522	67.5	71.0	37
	20200607	109.3	50.6	26

https://doi.org/10.5194/hess-2024-51
Preprint. Discussion started: 13 March 2024


Hydrology and Earth System Sciences
Discussions

4. Results

4.1 Calibration of parameters

4.1.1 Calibrated parameters of the DTDUH flow routing method

The core of the DUH was the calculation of the grid flow velocity. The parameters that need to be determined in Eq. (9) consist of k, S, I_c and γ, in which k was the velocity coefficient and was determined based on different underlying surface types or different flow states (Foda et al., 2017), as shown in Fig. 3(c) and Fig. 3(f). S was the grid cell slope of the study areas, which could be obtained from the DEM data of the target basin, as shown in Fig. 3(b) and Fig. 3(e). I_c was determined using hourly mean rainfall intensity of the target basin, and this parameter was 10 mm h^{-1} for the two study watersheds. Additionally, parameter γ reflected the influence of soil moisture content on the flow velocity. The parameter γ of soil moisture content was determined to be 0.5 to reflect the influence of soil moisture content on the flow velocity for the two basins (Yi et al., 2022). It is noteworthy that the raster size of the two basins were divided into 30 m × 30 m. The rationality of the TDUH in these two basins had been validated in our previous research (Yi and Chen, 2022; Yi et al., 2022), and thus was not calibrated in this study.

4.1.2 Calibrated parameters of runoff generation using the XAJ model

The XAJ model was adopted as the hydrological forecasting framework, in which the surface runoff routing module was replaced by three surface runoff routing methods, and the other modules remained unchanged within the XAJ model. The objective of this study was to explore the influence of spatial heterogeneity of the runoff generation on the UH for flood prediction, and thus the parameters of the runoff generation module kept unchanged. The calibrated and validation processes are as follows:

1) The parameters of the XAJ model were calibrated using the SCEUA method, where the surface

https://doi.org/10.5194/hess-2024-51
Preprint. Discussion started: 13 March 2024


Hydrology and Earth System Sciences
Discussions

runoff routing method was the linear reservoirs. In total, all the 32 flood events in the Longhu River basin and the Donshi River basin were used for the calibration of the XAJ + LR (linear reservoir) model without further dividing the validation period.

2) Then, the TDUH and DTDUH were derived, based on physical characteristics and rainfall intensities of watersheds. The parameters' determination method is given in Section 4.1.1. In order to verify the rationality of the TDUH and DTDUH routing methods, we calibrated XAJ+TDUH and XAJ+DTDUH models separately, and compared their performances with that of XAJ + LR model, as shown in Appendix (Fig. S1 and Fig. S2). Results show that the proposed method exhibits consistent or better performances compared with the LR routing method. Specifically, the DTDUH method performed best over the three methods for the Longhu River basin, and the time to peak error is significantly better than that of the LR method. While, for the Dongshi River basin, the performances of the LR method were slightly better than that of the proposed method, which could be the reason that the DTDUH was computed without the observed runoff, and there are various uncertainties in the conceptualization or implementation of the DTDUH.

3) Finally, the evapotranspiration module, runoff generation module and runoff separation module and their parameters obtained in Step 1) were not changed so as to discuss the performance of different runoff routing models, and the LR routing method was replaced with the TDUH and DTDUH, respectively. The XAJ model with calibrated parameters in Step 1) and TDUH as well as DTDUH were used for the validation of the XAJ + (TDUH and DTDUH) model. Since the parameters of the XAJ model were determined by the model combining with LR method, this calibration method would be more inclined to optimize the performance of XAJ + LR model. When combined with other runoff

https://doi.org/10.5194/hess-2024-51
Preprint. Discussion started: 13 March 2024


Hydrology and Earth System Sciences
Discussions
Open Access
EGU

routing models, the accuracy of results may be affected to some extent.

4.2 Computation of the DTDUH

The TDUH was derived referring to Yi et al. (2022) and the rationality of the TDUH has been validated. The derivations of the proposed DTDUH were similar to those of the TDUH. The main differences lied in that the DTDUH was derived for a specific saturated area. In order to obtain the DTDUHs corresponding to various saturated states of the watershed, the tension water storage in each grid cell within the basin was considered to be negatively correlated with the Topographic Wetness Index (TWI) (Shi et al., 2008; Tong et al., 2018; Yuan et al., 2019). We assumed topographic information captures the runoff generation heterogeneity at the catchment scale, and the TWI was used as an index to identify rainfall–runoff similarity (Beven and Kirkby, 1979). Areas with similar TWI values are regarded as possessing equal runoff generation potential. Specifically, the areas with larger TWI values tend to be saturated first and contribute to saturation excess rainfall; but the areas with lower TWI values need more water to reach saturation and generate runoff (Gao et al., 2019).

Then, the proposed distributed unit hydrographs (DTDUH) are computed based on the saturated areas, which can be expressed by TWI. When calculating discharge using the DTDUH, we should select various DTDUH based on the time-varying soil moisture within each time interval. Theoretically, the DTDUH is different at each time interval because α_t is ranging from 0 to 1. However, practically applying time-varying soil moisture based on DTDUH can be a complex task. In order to improve the effectiveness of the routing method, the soil moisture contents α_t in Eq. (9) were discretized to 0.25, 0.5, 0.75 and 1 based on the distributions of the TWI. Then, a simplified DTDUH can be obtained in a certain range soil moisture content. And these ranges are presented in Table 2. The distribution of the

https://doi.org/10.5194/hess-2024-51
Preprint. Discussion started: 13 March 2024

Hydrology and Earth System Sciences
Discussions
Open Access
EGU

345 saturated areas corresponding to different soil proportions are shown in Fig. 4. Similarly, the ratio of
346 excess rainfall intensity and the reference excess rainfall intensity $\frac{I_t}{I_c}$ in Eq. (9) were discretized to
347 0.5, 1, 1.5 and 2 in order to improve the calculation efficiency. More details can be found in Yi et al.
348 (2022).

349 **Table 2.** The soil moisture content α_t of each interval corresponds to the discrete soil moisture α_s.

Soil moisture α_t	$0 \leq \alpha_t \leq 0.25$	$0.25 < \alpha_t \leq 0.5$	$0.5 < \alpha_t \leq 0.75$	$0.75 < \alpha_t \leq 1$
Discrete soil moisture α_s	0.25	0.5	0.75	1

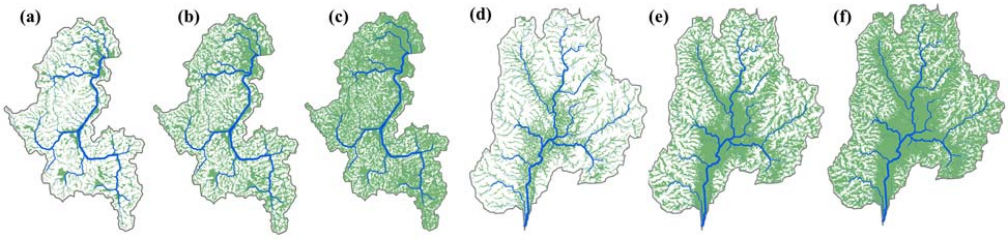

350

351 **Figure 4.** Saturated areas corresponding to various soil moisture proportions, where green area
352 represents the saturated region and white area represents the unsaturated region. (a), (b) and (c) are the
353 saturated areas corresponding to 0.25, 0.5 and 0.75 soil moisture proportions for the Longhu River
354 basin. (d), (e) and (f) are the saturated areas corresponding to 0.25, 0.5 and 0.75 soil moisture
355 proportions for the Dongshi River basin.

356 The computed TDUHs and DTDUHs for the Longhu River basin and the Dongshi River basin
357 are demonstrated in Fig. 5 to Fig. 8. For instance, when the excess rainfall intensities range from 0 to
358 5 mm h^{-1} and the soil moisture contents are between 0 and 0.25, the TDUH used for the surface runoff
359 routing is corresponding to the red line in Fig. 5(a) for the Longhu River basin. Although the time to
360 peak and flow peak discharge can be different for various TDUHs, the areas below the curve are the
361 same with each other. However, the areas below the curve are not necessary the same for the DTDUH,
362 as the proposed DTDUH is derived from the saturated areas, as shown in Fig. 6. Only when the
363 watershed reaches a global saturated state will the DTDUH be the same as the TDUH. It is noteworthy

https://doi.org/10.5194/hess-2024-51
Preprint. Discussion started: 13 March 2024

Hydrology and Earth System Sciences
Discussions

that for the same rainfall intensity, the time to peak of the DTDUHs corresponding to various soil moisture content are almost consistent with slight variations.

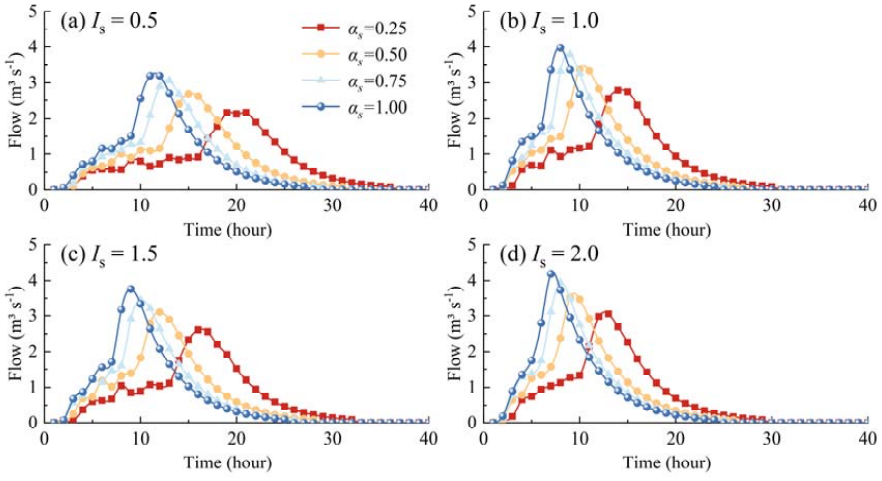

Figure 5. The TDUHs of the Longhu River basin. (a) I_s = 0.5. (b) I_s = 1.0. (c) I_s = 1.5. (d) I_s = 2.0.

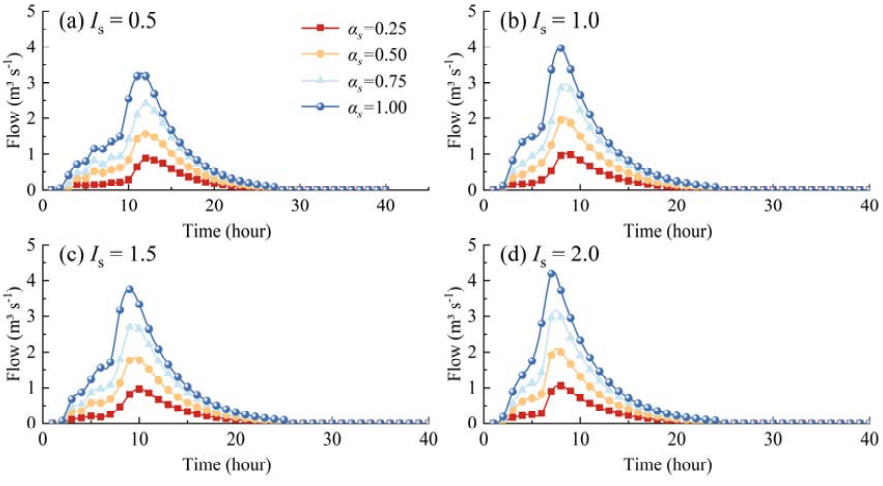

Figure 6. The DTDUHs of the Longhu River basin. (a) I_s = 0.5. (b) I_s = 1.0. (c) I_s = 1.5. (d) I_s = 2.0.

https://doi.org/10.5194/hess-2024-51
Preprint. Discussion started: 13 March 2024

Hydrology and Earth System Sciences
Discussions

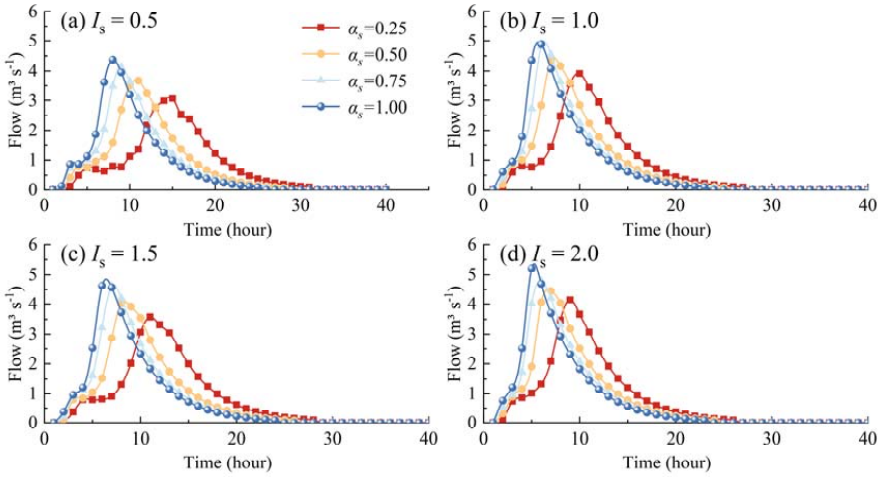

370

371 **Figure 7.** The TDUHs of the Dongshi River basin. (a) I_s = 0.5. (b) I_s = 1.0. (c) I_s = 1.5. (d) I_s = 2.0.

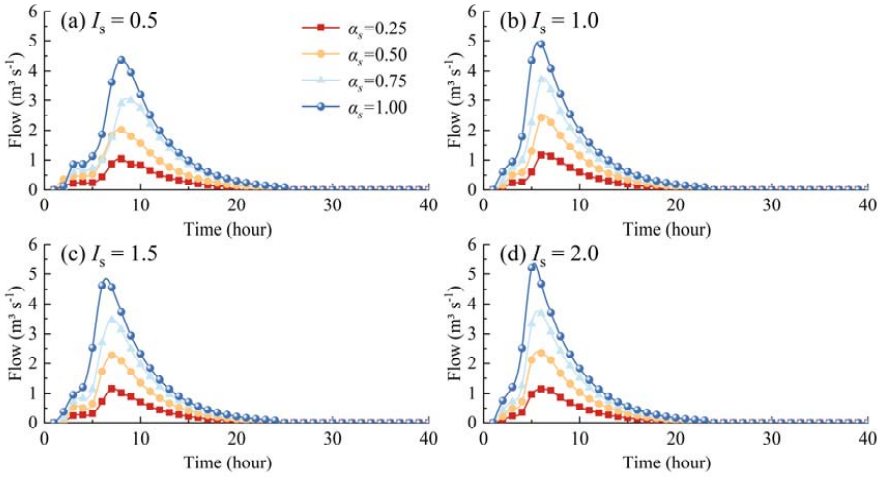

372

373 **Figure 8.** The DTDUHs of the Dongshi River basin. (a) I_s = 0.5. (b) I_s = 1.0. (c) I_s = 1.5. (d) I_s = 2.0.

374 *4.3 Errors due to spatial scale mismatch between runoff generation and runoff routing*

375 To investigate the possible errors due to spatial scale mismatch between runoff generation and
376 runoff routing, we assumed several sets of excess rainfall with intensities of 5, 10, 15 and 20 mm h^{-1},
377 and the saturated proportions of the basin are 0.25, 0.5, 0.75 and 1, respectively. Considering the
378 average rainfall intensities of the two basins, the time durations of the rainfall are assumed changing

https://doi.org/10.5194/hess-2024-51
Preprint. Discussion started: 13 March 2024


Hydrology and Earth System Sciences
Discussions

379 from 1 to 4 h, and the combinations are shown in the Table 3. Thus, 16 combinations can be formed
380 based on Table 3. For example, combination R-T1-S1 indicates there is a total depth of 20 mm excess
381 rainfall in the global watershed with the time duration being 1 hour (20 mm h^{-1}), and the saturated
382 proportion of the basin is 0.25. Similarly, combination R-T3-S2 indicates there is a total depth of 20
383 mm excess rainfall in the global watershed with the time durations being 4 hours (5 mm h^{-1}), and the
384 saturated proportion of the basin is 0.50. Then, the flow hydrograph due to the assumed excess rainfall
385 can be obtained using the TDUH and the DTDUH, thus to compare the errors of spatial scale mismatch
386 between runoff generation and runoff routing. The flow hydrograph computed using the TDUH and
387 DTDUH corresponding to the two basins are shown in Fig. 9 and Fig. 10, respectively.

388 **Table 3.** Combinations of the assumed excess rainfall, time duration and soil moisture content.

Depth of excess rainfall (mm)	Time duration (h)	Soil moisture content
20 (R)	1 (T1)	0.25 (S1)
20 (R)	2 (T2)	0.50 (S2)
20 (R)	3 (T3)	0.75 (S3)
20 (R)	4 (T4)	1.00 (S4)

https://doi.org/10.5194/hess-2024-51
Preprint. Discussion started: 13 March 2024

Hydrology and Earth System Sciences
Discussions

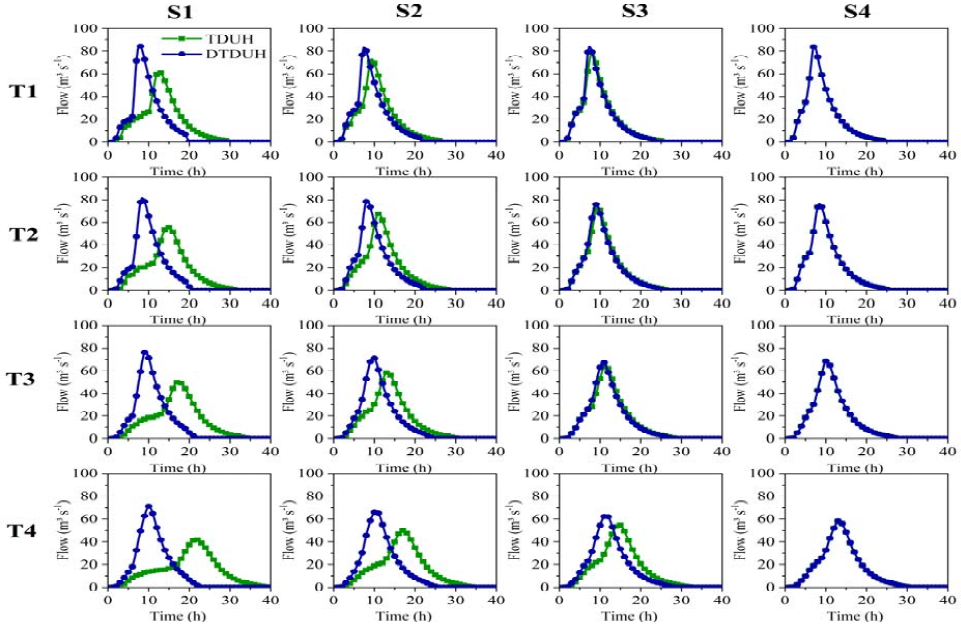

389

390 **Figure 9.** Errors of the flow hydrograph due to spatial mismatch between runoff generation and runoff

391 routing for the Longhu River basin

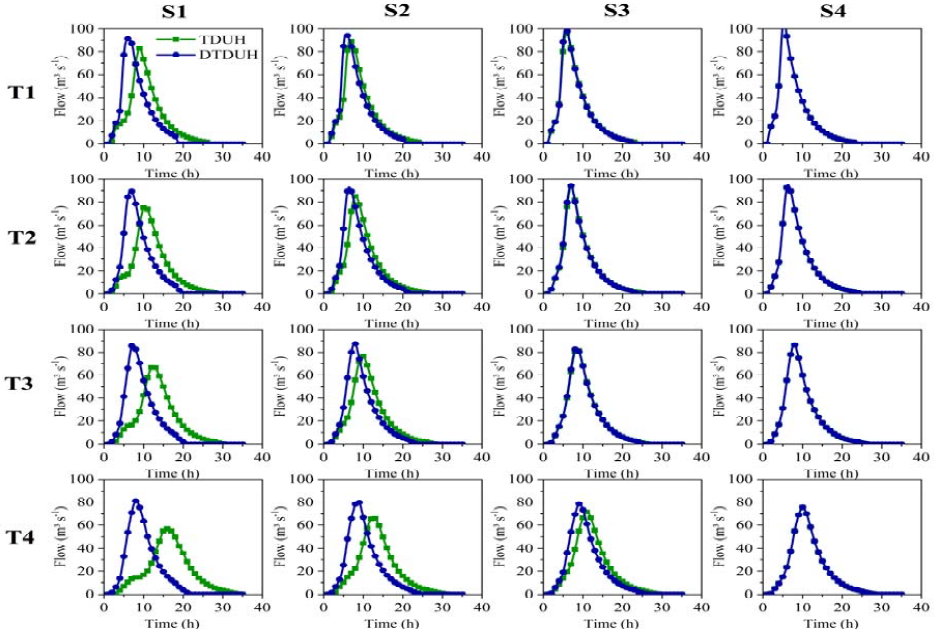

392

https://doi.org/10.5194/hess-2024-51
Preprint. Discussion started: 13 March 2024


Hydrology and Earth System Sciences
Discussions

393 **Figure 10.** Errors of the flow hydrograph due to spatial mismatch between runoff generation and runoff
394 routing for the Dongshi River basin

395 It can be found from Fig. 9 that the soil moisture significantly influences the results of the TDUH,
396 while the results of the DTDUH are almost not changed with the variation of soil moisture for the
397 Longhu River basin. When the saturated soil moisture proportion is low, the results of the two routing
398 methods are significantly different. Simultaneously, when the saturated soil moisture proportion
399 exceeds 0.5, the results of the TDUH and the DTDUH perform almost consistently. The differences
400 between the results of the two methods increase with the duration of excess rainfall.

401 For the Dongshi River basin, it can be seen from Fig. 10 that patterns of the soil moisture and
402 time duration on the performances are basically consistent with those of the Longhu River basin.
403 Conversely, the soil moisture shows a more pronounced effect on the DTDUH, and the flow peak
404 discharge become higher with the soil moisture changing from S1 to S4. It can also be found that the
405 differences between the results of the TDUH and the DTDUH in the Dongshi River basin are smaller
406 than those in the Longhu River basin, which means that the two routing methods will perform similarly
407 for the Dongshi River basin.

408 In summary, the performances of the TDUH and DTDUH are consistent for higher soil moisture
409 and higher rainfall intensity. When the soil moisture is low and the time duration of the excess rainfall
410 is long, we should pay much attention to the errors due to the spatial scale mismatch between runoff
411 generation and runoff routing. Additionally, the differences caused by this mismatch vary significantly
412 in different watersheds.

https://doi.org/10.5194/hess-2024-51
Preprint. Discussion started: 13 March 2024

Hydrology and Earth System Sciences
Discussions

4.4 Performances of the DTDUH for the Longhu River basin

A total of 16 isolated storms with the observed runoff responses from 1973 to 2016 were selected to explore the performances of the TDUH and DTDUH for the Longhu River basin. Since the TDUH and the DTDUH were used for the surface runoff routing, the proportions of the surface runoff had significant influence on the hydrological modelling performances. However, the performances of the model were evaluated based on the flow hydrograph at the outlet of the watershed, and the flow hydrograph was composed by three components including the surface runoff, subsurface stormflow runoff and subsurface runoff. To evaluate the performances of the TDUH and DTDUH under the condition of XAJ modelling framework, we are supposed to calculate the ratio of surface runoff to the total depth of excess rainfall, as shown in Fig. 11(a). Results show that the surface runoff accounts for most of the total depth of excess rainfall, which means that the performances of the hydrological model are mainly affected by the surface runoff routing methods. To this end, it is reasonable to compare the performances of the TDUH and DTDUH for the Longhu River basin. Simultaneously, Fig. 11(b) shows the antecedent soil moisture of the 16 flood events. The proportion of the saturated areas accounts more than 50% for most of the flood events.

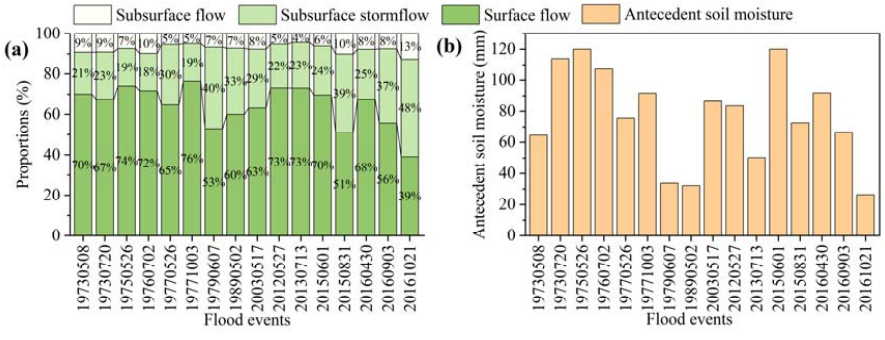

Figure 11. Details of the runoff components and antecedent soil moisture of the 16 flood events for

https://doi.org/10.5194/hess-2024-51
Preprint. Discussion started: 13 March 2024

Hydrology and Earth System Sciences
Discussions

the Longhu River basin. (a) Stacked bar charts of runoff components. (b) Bar charts of the antecedent soil moisture.

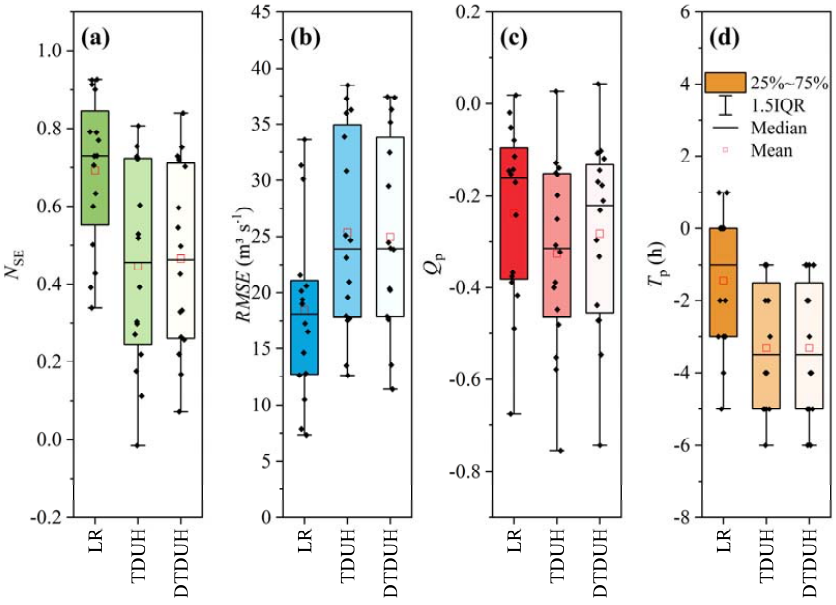

Figure 12. Distributions of the evaluation index based on different runoff routing methods for the Longhu River basin. (a) Distribution of *NSE*. (b) Distribution of *RMSE*. (c) Distribution of Q_p. (d) Distribution of T_p.

Three surface runoff routing methods were used for the runoff simulation. Fig. 12 plots the distributions of the evaluation index using different surface runoff routing methods. Results of the four indicators show that the average *NSE* of the two DUH methods were low since the parameters of the XAJ model were calibrated with the linear reservoir method, hence the linear reservoir method performed the best. The results of the TDUH and DTDUH were basically consistent, and the DTDUH performed slightly better than TDUH. Noteworthily, it can be seen form Fig. 12(c) that the median of the relative error of the flood peak of the DTDUH method is increased by 10% compared to that of the

https://doi.org/10.5194/hess-2024-51
Preprint. Discussion started: 13 March 2024


Hydrology and Earth System Sciences
Discussions

443 TDUH method, and the average error of the relative flood peak discharge of the proposed method is
444 significantly smaller than that of the TDUH. The average antecedent soil moisture of the Longhu River
445 basin is 77 mm which leads to a saturated proportion larger than 0.5. As discussed in the Section 4.2,
446 the performances of the TDUH and DTDUH are consistent when the saturated proportion is larger
447 than 0.5.

448 Additionally, we selected several flood events whose antecedent soil moisture are low and the
449 *NSE* is larger than 0.5 for analyses. Table 4 lists the evaluation indicators of the three methods in the
450 runoff forecasting application. It can be seen from Table 4 that all these four flood events show good
451 performances when the linear reservoir is used for the runoff routing. The antecedent soil moistures of
452 these flood events are 64, 33, 50 and 26 mm, respectively. The errors of the relative flood peak
453 discharge of the DTDUH decrease by 3%, 3%, 3% and 8% for the four flood events, compared with
454 those of the TDUH. The *NSE* of the TDUH and the DTDUH are consistent, and the *RMSE* of the
455 DTDUH is slightly lower than that of the TDUH methods. The time to flood peak is absolutely the
456 same for the two methods. It can be concluded that the DTDUH method indicates good performances
457 for the flood events with low antecedent soil moisture, and it performs consistently with the TDUH
458 when the global watershed is nearly saturated. This conclusion is consistent with that of the Section
459 4.2, and the assumption that there will be considerable errors due to the spatial scale mismatch between
460 runoff generation and runoff routing in low antecedent soil moisture, has been validated.

461 **Table 4.** Indicators of different routing methods for the Longhu River basin.

Indicators	Flood events	Linear reservoir	TDUH	DTDUH	Performances
NSE	19730508	0.93	0.81	0.84	↑
	19790607	0.73	0.60	0.60	–

https://doi.org/10.5194/hess-2024-51
Preprint. Discussion started: 13 March 2024

Hydrology and Earth System Sciences
Discussions

RMSE	20130713	0.91	0.72	0.70	↓
	20161021	0.90	0.72	0.72	−
	19730508	7.85	12.62	11.46	↑
	19790607	14.63	17.71	17.85	↓
	20130713	20.15	36.03	37.36	↓
	20161021	10.51	17.55	17.64	↓
Q_p	19730508	-0.15	-0.20	-0.17	↑
	19790607	-0.14	-0.14	-0.11	↑
	20130713	-0.05	-0.15	-0.12	↑
	20161021	-0.08	-0.25	-0.17	↑
T_p	19730508	0	-4	-4	−
	19790607	0	-2	-2	−
	20130713	0	-1	-1	−
	20161021	-3	-5	-5	−

Note: The symbols ↑, ↓ and − mean the performance of the DTDUH is better, lower and consistent compared with that of the TDUH.

4.5 Performances of the DTDUH for the Dongshi River basin

Similarly, a total of 16 isolated storms with the observed runoff responses from 2015 to 2020 were selected to explore the performances of the TDUH and DTDUH for the Dongshi River basin. The components of the runoff and the antecedent soil moisture for the 16 flood events are shown in Fig. 13(a) and Fig. 13(b). Fig. 13(a) shows that the depth of the surface runoff accounts for more than 70% of the total depth runoff and the study watershed has no subsurface stormflow, which means that the Dongshi River basin can also be well used for exploring the performances of the TDUH and the DTDUH. The average antecedent soil moisture of the 16 flood events is 87 mm, which is larger than that of the Longhu River basin.

Fig. 14 plots the distributions of the evaluation index using different flow routing methods for the Dongshi River basin. It can be seen from Fig. 14 that the linear reservoir method shows the best performances overall, and the TDUH and DTDUH have consistent performances. The consistent

https://doi.org/10.5194/hess-2024-51
Preprint. Discussion started: 13 March 2024

Hydrology and Earth System Sciences
Discussions

476 performances of the TDUH and DTDUH can be due to the fact that the average antecedent soil
477 moisture of these 16 flood events is high. Hence, the errors caused by the spatial scale mismatch are
478 small.

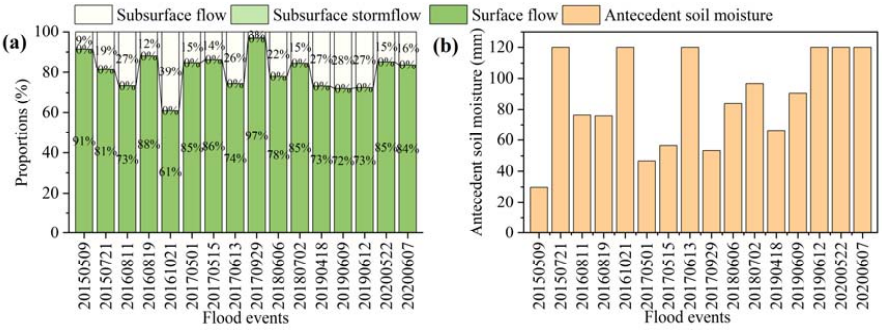

479

480 **Figure 13.** Details of the runoff components and antecedent soil moisture of the 16 flood events for
481 the Dongshi River basin. (a) Stacked bar charts of runoff components. (b) Bar charts of the antecedent
482 soil moisture.

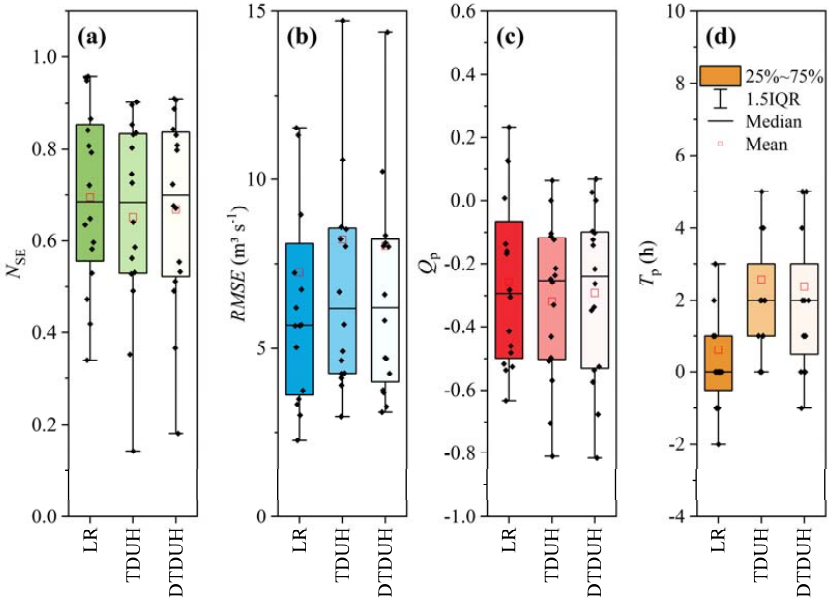

483

484 **Figure 14.** Distributions of the evaluation index based on different runoff routing methods for the

https://doi.org/10.5194/hess-2024-51
Preprint. Discussion started: 13 March 2024

Hydrology and Earth System Sciences
Discussions

485 Dongshi River basin. (a) Distribution of *NSE*. (b) Distribution of *RMSE*. (c) Distribution of Q_p. (d)
486 Distribution of T_p.

487 However, the differences of the results of the TDUH and DTDUH can be identified in specific
488 flood event. Table 5 lists the evaluation indicators of the three methods in the runoff forecasting
489 application for flood events No. 20170501, No. 20170515, No. 20170929 and No. 20190418. The
490 antecedent soil moistures of these flood events are 47, 56, 53 and 66 mm, respectively. It can be found
491 from Table 5 that the performances of the DTDUH are better than those of the TDUH. Therefore, we
492 can conclude that the proposed DTDUH shows higher accuracy for the flood events with lower
493 antecedent soil moisture, and these results are the same with those of the Longhu River basin.

494 **Table 5.** Indicators of different routing methods for the Dongshi River basin.

Indicators	Flood events	Linear reservoir	TDUH	DTDUH	Performances
NSE	20170501	0.87	0.64	0.67	↑
	20170515	0.72	0.59	0.68	↑
	20170929	0.42	0.73	0.81	↑
	20190418	0.64	0.53	0.55	↑
RMSE	20170501	3.01	4.91	4.71	↑
	20170515	3.49	4.25	3.75	↑
	20170929	5.67	3.90	3.25	↑
	20190418	7.24	8.23	8.01	↑
Q_p	20170501	-0.28	-0.26	-0.10	↑
	20170515	0.12	-0.12	-0.10	↑
	20170929	0.23	-0.43	0.067	↑
	20190418	-0.52	-0.70	-0.68	↑
T_p	20170501	0	4	0	↑
	20170515	0	4	4	–
	20170929	-2	2	1	↑
	20190418	1	2	2	–

495 *Note: The symbols ↑, ↓ and – mean the performance of the DTDUH is better, lower and*
496 *consistent compared with that of the TDUH.*

https://doi.org/10.5194/hess-2024-51
Preprint. Discussion started: 13 March 2024

Hydrology and Earth System Sciences
Discussions

5. Discussion

5.1 Forecasting performance advantage analysis of the proposed DTDUH

There is no issue on the spatial scale mismatch between runoff generation and runoff routing in the fully distributed hydrological model, since the fully distributed model solves the St. Venant equations, however, they are usually computationally intensive (Bunster et al., 2019). For the conceptual models, the spatially DUH method is an alternative method that allows the use of distributed information in a much more efficient manner. A novel DUH method was proposed in this study for the surface runoff routing, namely the DTDUH. The proposed DTDUH was computed based on the runoff generation areas instead of the whole basin. This realization was significant different with the current understandings (Gibbs et al., 2010; Goñi et al., 2019; Andrieu et al., 2021). To this end, the TDUH and the DTDUH can be used for exploring the influence of spatial heterogeneity of runoff generation on the runoff routing. The differences of the definition, assumptions as well as limitations between the current theory and the DTDUH have been concluded in Table 6.

Table 6. The differences of the definition, assumptions as well as limitations between the current theory and the DTDUH.

Differences	Current theory	DTDUH
Definition	A typical hydrograph of direct runoff which gets generated from one centimetre of effective rainfall falling at a uniform rate over the entire drainage basin uniformly during a specific duration.	A typical hydrograph of direct runoff which gets generated from one centimetre of effective rainfall falling at a uniform rate over the saturated drainage basin uniformly during a specific duration.
Assumption	i) The effective rainfall is uniformly distributed over the entire drainage basin. ii) The effective rainfall occurs uniformly within its specifier duration. iii) The principle time invariance.	i) The effective rainfall is uniformly distributed over the saturated drainage areas. ii) The effective rainfall occurs uniformly within its specifier duration.

https://doi.org/10.5194/hess-2024-51
Preprint. Discussion started: 13 March 2024

Hydrology and Earth System Sciences
Discussions

		iii) It can be time variant.
Limitation	i) The limiting size of the drainage basin is considered to be 5000 km^2. ii) The physical basin characteristics must be unchanged.	i) The limiting size of the drainage basin is small watershed, otherwise the DUH method is not applicable. ii) The saturated areas should be obtained based on the physical characteristics of the watershed.

In this study, the DTDUH was computed considering the time-varying characteristics of the saturated areas, and the excess rainfall was redistributed in the saturated areas instead of the whole basin. The diagram of the DTDUH derivation processes corresponding to various saturated soil moisture can be shown as Fig. 15. The total travel time from each saturated grid cell to the outlet is obtained by directly recording each particle's total travel time from the initial location until the particle leaves the basin. We can obtain the DTDUH when the last particle leaves the basin. There are 24 grid cells in the basin. For instance, the derivation of the TDUH corresponding to saturated proportions 25% (6 grid cells) is shown as Fig. 15(a). The DTDUH is not the same with the TDUH until the basin reach a global saturation as Fig. 15(d).

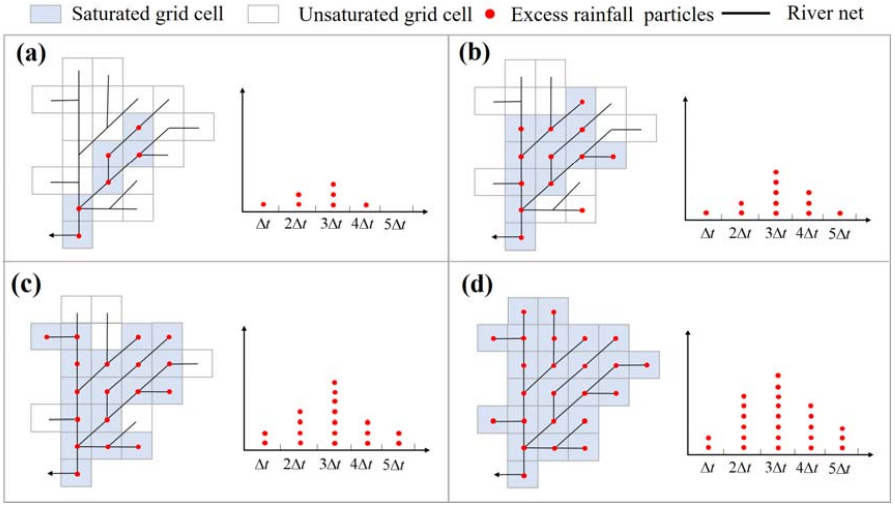

Figure 15. The diagram of the DTDUH corresponding to various soil moisture. (a) $\alpha_s = 0.25$. (b)

https://doi.org/10.5194/hess-2024-51
Preprint. Discussion started: 13 March 2024


Hydrology and Earth System Sciences
Discussions

523 $\alpha_s = 0.50$. (c) $\alpha_s = 0.75$. (d) $\alpha_s = 1.00$.

524 For instance, when there occurs a stormflow with the depth of 10 mm in the whole basin and the
525 saturated proportion is 50%, the actual depth of the excess rainfall in the saturated area is 20 mm. In
526 tradition, the flow hydrograph was calculated using the TDUH as Fig 15. (d), neglecting the issues that
527 excess rainfall particles are only on the saturated areas. This neglection therefore leads to errors
528 because the unsaturated areas where no excess rainfall is generated contributes to the confluence. To
529 solve this issue, the flow hydrograph was calculated using the DTDUH as Fig. 15 (b) in this study, and
530 in turn can improve the forecast performances of the hydrological model.

531 *5.2 Potential shortcomings and improvements of the proposed DTDUH*

532 Although the performances of the DTDUH methods are better than those of the TDUH methods,
533 there are still some issues that need to be addressed: 1) A hybrid runoff generation process pattern
534 formed by more than one mechanism can often be identified in semi-humid, semi-arid and mountain
535 watershed, because of the heterogeneity of underlying surface conditions and meteorological factors
536 (Hu et al., 2021; Yi et al., 2023). When there occurs more than the saturation-excess rainfall, the
537 saturated area extraction method based on the TWI will not be applicable as the excess rainfall can
538 also be generated from the unsaturated areas; 2) As discussed above, the saturation areas were extracted
539 based on the TWI in this study (Tong et al., 2018; Yuan et al., 2019). When the rainfall is spatially
540 uneven distributed over the watershed, the errors of the extracted saturated area can be huge as the gird
541 cells with larger tension water capacity may be saturated in a shorter time than those with smaller
542 tension water capacity. Thus, determining the time-varying saturated grid cells is a considerable
543 challenge for the accurate hydrological forecasting, since it influences the accuracy of the DTDUH; 3)

https://doi.org/10.5194/hess-2024-51
Preprint. Discussion started: 13 March 2024

544 The DTDUH can be well used for the areas with abundant surface runoff. For the semi-humid and
545 semi-arid watershed with a large proportion of the subsurface stormflow runoff and subsurface runoff,
546 how to develop a dynamic confluence method suitable for these regions is another challenging
547 hydrologic issue because the mechanism of the subsurface stormflow generation is ambiguous, and
548 quantifying the subsurface stormflow generating processes is a formidable task as the subsurface
549 stormflow runoff and subsurface runoff cannot be observed directly.

550 6. Conclusions

551 A novel DTDUH method was proposed to explore the influence of spatial heterogeneity of runoff
552 generation on the runoff routing. The XAJ model was used as the hydrological modelling framework.
553 The Longhu River basin and the Dongshi River basin were selected as two case studies. The results of
554 the three surface runoff routing methods including the linear reservoir, TDUH and DTDUH were
555 compared. The advantages and shortcomings of the proposed method have been discussed. The main
556 conclusions can be summarized as follows:

557 1. A novel DTDUH method designed for the surface runoff routing was proposed based on the
558 TDUH method. The traditional TDUH method was derived based on the whole basin, and the proposed
559 method was designed only for the saturated areas. The DTDUH method considered not only the time-
560 varying rainfall intensities and soil moisture, but also the time-varying saturated areas of the watershed
561 which were extracted based on the TWI.

562 2. The rationality of the proposed method was verified by comparing the performances of
563 XAJ+LR, XAJ + TDUH and XAJ +DTDUH models, which were calibrated separately. Results shows
564 that the proposed method exhibited consistent or better performance compared with that of the LR

https://doi.org/10.5194/hess-2024-51
Preprint. Discussion started: 13 March 2024

routing method, and performed better than the TDUH method.

3. The influence of spatial heterogeneity of runoff generation on the runoff routing was carried out by comparing the performances of the TDUH and the DTDUH. The performances of the proposed DTDUH has been compared with the traditional TDUH method in the Longhu River basin and the Dongshi River basin while the parameters of the runoff generation module remained the same. Results show that the DTDUH show a better performance for the flood events with low antecedent soil moisture, and when the antecedent soil moisture is high, the performance of the two methods performed consistently.

4. The differences of definition, assumptions as well as limitations between the current UH theory and the DTDUH have been discussed. Additionally, some challenges related to the DTDUH has been presented, for example, the hybrid runoff being generated more than in the saturated areas, the extraction accuracy of the time-varying saturation areas, and the spatial scale mismatch between runoff generation and runoff routing of the subsurface stormflow runoff as well as the subsurface runoff.

https://doi.org/10.5194/hess-2024-51
Preprint. Discussion started: 13 March 2024


Hydrology and Earth System Sciences
Discussions

Data availability

Due to the strict security requirements from the departments, some or all data, models, or code generated or used in the study are proprietary or confidential in nature and may only be provided with restrictions (e.g. anonymized data).

Author contributions

Lu Chen conceived the original idea, and Bin Yi designed the methodology, developed the code and performed the study. Lu Chen, Bin Yi and Tao Xie contributed to the interpretation of the results. Bin Yi wrote the paper, and Lu Chen revised the paper.

Competing interests

The authors declare that they have no conflict of interest.

Acknowledgments

This study was financially supported by the National Key R&D Program of China (2023YFC3081000, 2021YFC3200400), and the Science and Technology Plan Projects of Tibet Autonomous Region (XZ202301YD0044C).

References

Andrieu, H., Moussa, R., Kirstetter, P.-E., 2021. The Event-specific Geomorphological Instantaneous Unit Hydrograph (E-GIUH): The basin hydrological response characteristic of a flood event. Journal of Hydrology, 603: 127158. https://doi.org/10.1016/j.jhydrol.2021.127158.

Beven, K. J., Kirkby, M. J., 1979. A physically based, variable contributing area model of basin hydrology / Un modèle à base physique de zone d'appel variable de l'hydrologie du bassin versant. Hydrological Sciences Bulletin, 24(1): 43-69. https://doi.org/10.1080/02626667909491834.

Boughton, W., 2004. The Australian water balance model. Environmental Modelling & Software, 19(10): 943-956. https://doi.org/10.1016/j.envsoft.2003.10.007.

Brunner, M. I., Swain, D. L., Wood, R. R., Willkofer, F., Done, J. M., Gilleland, E., Ludwig, R., 2021. An extremeness threshold determines the regional response

https://doi.org/10.5194/hess-2024-51
Preprint. Discussion started: 13 March 2024

of floods to changes in rainfall extremes. Communications Earth & Environment, 2(1): 173. https://doi.org/10.1038/s43247-021-00248-x.

Bunster, T., Gironás, J., Niemann, J. D., 2019. On the influence of upstream flow contributions on the basin response function for hydrograph prediction. Water Resources Research, 55(6): 4915-4935. https://doi.org/10.1029/2018WR024510.

Cho, Y., Engel, B. A., Merwade, V. M., 2018. A spatially distributed Clark's unit hydrograph based hybrid hydrologic model (Distributed-Clark). Hydrological Sciences Journal, 63(10): 1519-1539. https://doi.org/10.1080/02626667.2018.1516042.

Clark, C. O., 1945. Storage and the Unit Hydrograph. Transactions of the American Society of Civil Engineers, 110(1): 1419-1446. https://doi.org/10.1061/TACEAT.0005800.

Czyzyk, K., Mirossi, D., Abdoulhak, A., Hassani, S., Niemann, J. D., Gironás, J., 2020. Impacts of Channel Network Type on the Unit Hydrograph. Water, 12(3): 669. https://doi.org/10.3390/w12030669.

Du, J., Xie, H., Hu, Y., Xu, Y., Xu, C.-Y., 2009. Development and testing of a new storm runoff routing approach based on time variant spatially distributed travel time method. Journal of Hydrology, 369(1-2): 44-54. https://doi.org/10.1016/j.jhydrol.2009.02.033.

Duan, Q., Sorooshian, S., Gupta, V., 1992. Effective and efficient global optimization for conceptual rainfall - runoff models. Water Resources Research, 28(4): 1015-1031. https://doi.org/10.1029/91WR02985.

Foda, R. F., Awadallah, A. G., Gad, M. A., 2017. A Fast Semi Distributed Rainfall Runoff Model for Engineering Applications in Arid and Semi-Arid Regions. Water Resources Management, 31(15): 4941-4955. https://doi.org/10.1007/s11269-017-1787-2.

Gao, H., Birkel, C., Hrachowitz, M., Tetzlaff, D., Soulsby, C., Savenije, H. H. G., 2019. A simple topography-driven and calibration-free runoff generation module. Hydrology and Earth System Sciences, 23(2): 787-809. 10.5194/hess-23-787-2019.

Gibbs, M., Dandy, G., Maier, H., 2010. Evaluation of parameter setting for two GIS based unit hydrograph models. Journal of Hydrology, 393(3-4): 197-205. https://doi.org/10.1016/j.jhydrol.2010.08.014.

Goñi, M., López, J. J., Gimena, F. N., 2019. Geomorphological instantaneous unit hydrograph model with distributed rainfall. CATENA, 172: 40-53. https://doi.org/10.1016/j.catena.2018.08.010.

Goodrich, D. C., Lane, L. J., Shillito, R. M., Miller, S. N., Syed, K. H., Woolhiser, D. A., 1997. Linearity of basin response as a function of scale in a semiarid watershed. Water Resources Research, 33(12): 2951-2965. https://doi.org/10.1029/97WR01422.

Gray, D. M., 1961. Synthetic Unit Hydrographs for Small Watersheds. Journal of the

https://doi.org/10.5194/hess-2024-51
Preprint. Discussion started: 13 March 2024

Hydraulics Division, 87(4): 33-54. https://doi.org/10.1061/JYCEAJ.0000631.

Grimaldi, S., Petroselli, A., Alonso, G., Nardi, F., 2010. Flow time estimation with spatially variable hillslope velocity in ungauged basins. Advances in Water Resources, 33(10): 1216-1223. https://doi.org/10.1016/j.advwatres.2010.06.003.

Grimaldi, S., Petroselli, A., Nardi, F., 2012. A parsimonious geomorphological unit hydrograph for rainfall–runoff modelling in small ungauged basins. Hydrological Sciences Journal, 57(1): 73-83. https://doi.org/10.1080/02626667.2011.636045.

Gupta, V. K., Waymire, E., Wang, C. T., 1980. A representation of an instantaneous unit hydrograph from geomorphology. Water Resources Research, 16(5): 855-862. https://doi.org/10.1029/WR016i005p00855.

Hoang, L., Schneiderman, E. M., Moore, K. E. B., Mukundan, R., Owens, E. M., Steenhuis, T. S., 2017. Predicting saturation-excess runoff distribution with a lumped hillslope model: SWAT-HS. Hydrological Processes, 31(12): 2226-2243. https://doi.org/10.1002/hyp.11179.

Hu, C. H., Ran, G., Li, G., Yu, Y., Wu, Q., Yan, D. H., Jian, S. Q., 2021. The effects of rainfall characteristics and land use and cover change on runoff in the Yellow River basin, China. Journal of Hydrology and Hydromechanics, 69(1): 29-40. https://doi.org/10.2478/johh-2020-0042.

Huang, Q., Qin, G., Zhang, Y., Tang, Q., Liu, C., Xia, J., Chiew, F. H. S., Post, D., 2020. Using Remote Sensing Data-Based Hydrological Model Calibrations for Predicting Runoff in Ungauged or Poorly Gauged Catchments. Water Resources Research, 56(8): e2020WR028205. https://doi.org/10.1029/2020WR028205.

Kirkby, M. J., 1976. Tests of the random network model, and its application to basin hydrology. Earth Surface Processes, 1(3): 197-212. https://doi.org/10.1002/esp.3290010302.

Lee, K. T., Chen, N.-C., Chung, Y.-R., 2008. Derivation of variable IUH corresponding to time-varying rainfall intensity during storms/Dérivation d'un HUI variable correspondant à l'évolution temporelle de l'intensité pluviométrique durant les averses. Hydrological Sciences Journal, 53(2): 323-337. https://doi.org/10.1623/hysj.53.2.323.

Li, H. Y., Sivapalan, M., 2014. Functional approach to exploring climatic and landscape controls on runoff generation: 2 Timing of runoff storm response. Water Resources Research, 50(12): 9323-9342. https://doi.org/10.1002/2014wr016308.

Liang, X., Lettenmaier, D. P., Wood, E. F., Burges, S. J., 1994. A simple hydrologically based model of land surface water and energy fluxes for general circulation models. Journal of Geophysical Research: Atmospheres, 99(D7): 14415-14428. https://doi.org/10.1029/94JD00483.

Maidment, D. R., Olivera, F., Calver, A., Eatherall, A., Fraczek, W., 1996. Unit Hydrograph Derived from a Spatially Distributed Velocity Field. Hydrological

689 Processes, 10(6): 831-844. https://doi.org/10.1002/(SICI)1099-
690 1085(199606)10:6<831::AID-HYP374>3.0.CO;2-N.
691 Martinez, V., Garcia, A., Ayuga, F., 2002. Distributed routing techniques developed on
692 GIS for generating synthetic unit hydrographs. Transactions of the ASAE, 45(6):
693 1825. https://doi.org/10.13031/2013.11433.
694 Melesse, A. M., Graham, W. D., 2004. Storm runoff prediction based on a spatially
695 distributed travel time method utilizing remote sensing and GIS. Journal of the
696 American Water Resources Association, 40(4): 863-879.
697 https://doi.org/10.1111/j.1752-1688.2004.tb01051.x.
698 Minshall, N. E., 1960. Predicting storm runoff on small experimental watersheds.
699 Journal of the Hydraulics Division, 86(8): 17-38
700 Monajemi, P., Khaleghi, S., Maleki, S., 2021. Derivation of instantaneous unit
701 hydrographs using linear reservoir models. Hydrology Research, 52(2): 339-
702 355. https://doi.org/10.2166/nh.2021.171.
703 Moore, R. J., 2007. The PDM rainfall-runoff model. Hydrol. Earth Syst. Sci., 11(1):
704 483-499. https://doi.org/10.5194/hess-11-483-2007.
705 Noto, L. V., La Loggia, G., 2007. Derivation of a distributed unit hydrograph integrating
706 GIS and remote sensing. Journal of Hydrologic Engineering, 12(6): 639-650.
707 https://doi.org/10.1061/(Asce)1084-0699(2007)12:6(639).
708 Paul, P. K., Kumari, N., Panigrahi, N., Mishra, A., Singh, R., 2018. Implementation of
709 cell-to-cell routing scheme in a large scale conceptual hydrological model.
710 Environmental Modelling & Software, 101: 23-33.
711 https://doi.org/10.1016/j.envsoft.2017.12.003.
712 Rigon, R., Bancheri, M., Formetta, G., De Lavenne, A., 2016. The geomorphological
713 unit hydrograph from a historical - critical perspective. Earth Surface Processes
714 Landforms, 41(1): 27-37. https://doi.org/10.1002/esp.3855.
715 Rodríguez-Iturbe, I., González-Sanabria, M., Bras, R. L., 1982. A geomorphoclimatic
716 theory of the instantaneous unit hydrograph. Water Resources Research, 18(4):
717 877-886. https://doi.org/10.1029/WR018i004p00877.
718 Rodríguez-Iturbe, I., Valdés, J. B., 1979. The geomorphologic structure of hydrologic
719 response. Water Resources Research, 15(6): 1409-1420.
720 https://doi.org/10.1029/WR015i006p01409.
721 Sarangi, A., Madramootoo, C. A., Enright, P., Prasher, S. O., 2007. Evaluation of three
722 unit hydrograph models to predict the surface runoff from a Canadian watershed.
723 Water Resources Management, 21(7): 1127-1143.
724 https://doi.org/10.1007/s11269-006-9072-9.
725 Seo, Y., Park, S. Y., Schmidt, A. R., 2016. Implication of the flow resistance formulae
726 on the prediction of flood wave propagation. Hydrological Sciences Journal,
727 61(4): 683-695. https://doi.org/10.1080/02626667.2014.992787.
728 Shi, P., Rui, X. F., Qu, S. M., Chen, X., 2008. Calculating storage capacity with
729 topographic index. Advances in Water Science, 19(2): 264-267
730 Snyder, F. F., 1938. Synthetic unit-graphs. Eos, Transactions American Geophysical

https://doi.org/10.5194/hess-2024-51
Preprint. Discussion started: 13 March 2024

Union, 19(1): 447-454. https://doi.org/10.1029/TR019i001p00447.

Tong, B., Li, Z., Yao, C., Wang, J., Huang, Y., 2018. Derivation of the Spatial Distribution of Free Water Storage Capacity Based on Topographic Index. Water, 10(10): 1407. https://doi.org/10.3390/w10101407.

Tromp-Van Meerveld, H. J., Mcdonnell, J. J., 2006. Threshold relations in subsurface stormflow: 1. A 147-storm analysis of the Panola hillslope. Water Resources Research, 42(2): W02411. https://doi.org/10.1029/2004wr003778.

Yi, B., Chen, L., 2022. A time-varying distributed unit hydrograph method considering dynamic flow routing path. Advances in Water Science, 33(6): 944-954. https://doi.org/10.14042/j.cnki.32.1309.2022.06.009.

Yi, B., Chen, L., Liu, Y., Guo, H., Leng, Z., Gan, X., Xie, T., Mei, Z., 2023. Hydrological modelling with an improved flexible hybrid runoff generation strategy. Journal of Hydrology, 620: 129457. https://doi.org/10.1016/j.jhydrol.2023.129457.

Yi, B., Chen, L., Zhang, H., Singh, V. P., Jiang, P., Liu, Y., Guo, H., Qiu, H., 2022. A time-varying distributed unit hydrograph method considering soil moisture. Hydrology and Earth System Sciences, 26(20): 5269-5289. https://doi.org/10.5194/hess-26-5269-2022.

Yuan, F., Zhang, L., Soe, K. M., Ren, L., Zhao, C., Zhu, Y., Jiang, S., Liu, Y., 2019. Applications of TRMM- and GPM-Era Multiple-Satellite Precipitation Products for Flood Simulations at Sub-Daily Scales in a Sparsely Gauged Watershed in Myanmar. Remote Sensing, 11(2): 140. https://doi.org/10.3390/rs11020140.

Zhao, R. J., 1992. The Xinanjiang model applied in China. Journal of Hydrology, 135(1): 371-381. https://doi.org/10.1016/0022-1694(92)90096-E.

Zhao, R. J., Zuang, Y. L., Fang, L. R., Liu, X. R., 1980. The Xinanjiang model[C]//Proceedings of the Oxford Symposium: 351-356. https://doi.org/10.1016/0022-1694(92)90096-E.

Zhou, Q., Chen, L., Singh, V. P., Zhou, J., Chen, X., Xiong, L., 2019. Rainfall-runoff simulation in karst dominated areas based on a coupled conceptual hydrological model. Journal of Hydrology, 573: 524-533. https://doi.org/10.1016/j.jhydrol.2019.03.099.